Joining 5754 Automotive Aluminum Alloy 2-mm-Thick Sheets Using Ultrasonic Spot Welding

When a peak temperature of above 500°C was attained, the material softened considerably, enhancing the joining of the aluminum sheets

BY C. Y. ZHANG, D. L. CHEN, AND A. A. LUO

ABSTRACT

The aim of this study was to evaluate the weldability and tensile shear failure load of a 2-mm-thick 5754 aluminum alloy sheet (a typical automotive structural material) joined via ultrasonic spot welding at various energy levels from about 2300 to 5800 J. The temperature changes at the weld center were monitored during welding. It was observed that the temperature rise rate and peak temperature increased rapidly with increasing welding energy. At an energy level between about 5000 and 5500 J, a peak temperature of more than 500°C was reached, leading to significant softening of the sheets required for proper joining, and a failure load of over 4 kN was achieved. With increasing welding energy, the interface was observed to change from a wavy line with some characteristic tree-like bifurcation to discontinuous voids or cracks, and to complete disappearance, corresponding to a progressively expanding joining area from the periphery to the center of the weld and an increasing tensile shear failure load.

Introduction

Ultrasonic spot welding (USW) is a solid-state process in which two sheet materials are joined by the application of ultrasonic vibrations at a frequency of ~20 kHz and an amplitude of 20–75 µm under a moderate pressure, where the vibrations are applied parallel to the interface between the sheets (Refs. 1–4). A solid-state weld can be achieved via a high-frequency relative motion between the sheets, coupled with severe plastic deformation and mechanical interlocking, as well as a chemical bond involving diffusion (Refs. 5–8). Compared with resistance spot welding, USW can join aluminum car body panels at lower energy consumption, using only 0.6–1.3 kJ per weld, and create a more homogeneous microstructure characterized by refined grains and confined inclusions free from pores between the base materials (Refs. 9, 10). In addition, USW requires no welding wire or water cooling, has modest space requirements, and results in no arcs or sparks. Therefore, USW is an alternative method that can be applied for joining aluminum (Al) alloys in automotive body construction (Refs. 1, 3).

During USW, welding energy is a key parameter for the welding of Al alloy sheets, as well as their mechanical properties. The previous USW system was only able to join thin foils, generally <0.5 mm in thickness, because of its lower power output (Ref. 11). For thicker sheets (1–2 mm), higher power welding systems are necessary (Refs. 3, 12). At a lower level of welding energy, the microbond density was too low; failure occurred through the interface. Higher welding energies can effectively promote joining in the entire weld, thus improving weld strength. Jahn et al. (Ref. 13) evaluated the effects of welding energy on the microstructure and weld strength of ultrasonic spot welds of AA6111-T4 Al alloy using a single-transducer, unidirectional wedge-reed welding machine. It was observed that the weld strength increased with increasing welding energy up to ~500 J, and the maximum failure load obtained was between 2.6 and 3.1 kN. Recently, Bakavos and Prangnell (Ref. 14) studied the joining mechanisms and microstructure formation in a high-power ultrasonic spot welded 6111 Al sheet. Good mechanical properties for the welds were obtained with a shear failure load of up to 3.5 kN. Strong welds could be achieved only after the welding energy exceeded a threshold; then a failure mode of button pullout occurred. The welding energy required during USW is closely related to the clamping pressure, welding time, as well as the vibration frequency (Refs. 15, 16). The welding energy and/or welding time can be reduced as the clamping pressure increases (Ref. 17). The mechanical properties are also related to the weldability of the materials to be welded. The lower the hardness, the more efficient the transfer of the welding energy (Ref. 17). Accompanied by the ultrasonic vibration, the input power leads to the temperature rise in the specimen. Therefore, how the temperature increases during USW becomes an important parameter to investigate the welding mechanisms (Refs. 18, 19). The specimen temperature, due to the friction dissipation at the weld interface during USW, generally arrives at 31~75% of the melting temperature. Doumanidis and Gao (Ref. 20) studied the USW process of a 0.127-mm-thick 1100 Al alloy experimentally and numerically. The thermal distribution during

C. Y. ZHANG (cyzhang@nwpu.edu.cn) *and D. L. CHEN* (dchen@ryerson.ca) *are with Dept. of Mechanical and Industrial Engineering, Ryerson University, Toronto, Ont., Canada. ZHANG is also with Science and Technology on Thermostructural Composite Materials Laboratory, Northwestern Polytechnical University, Xi'an, People's Republic of China. A. A. LUO is with Dept. of Materials Science and Engineering, Dept. of Integrated Systems Engineering, The Ohio State University, Columbus, Ohio.*

KEYWORDS

Ultrasonic Spot Welding
Aluminum Alloy
Tensile Shear
Temperature Monitoring

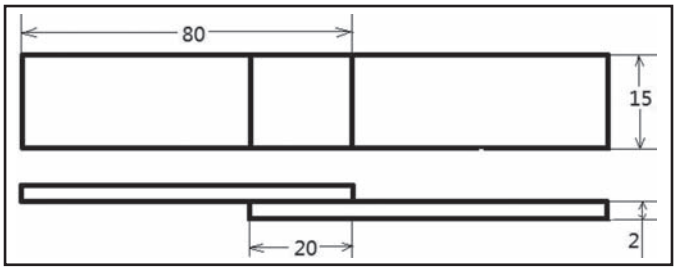

Fig. 1 — Schematic illustration of a test coupon used in the present ultrasonic spot welding.

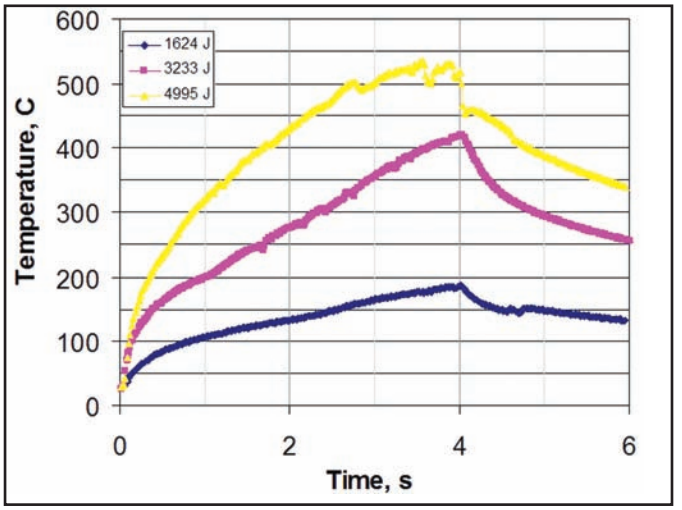

Fig. 3 — Variation of temperature at the center of the weld with time during USW at different levels of welding energy.

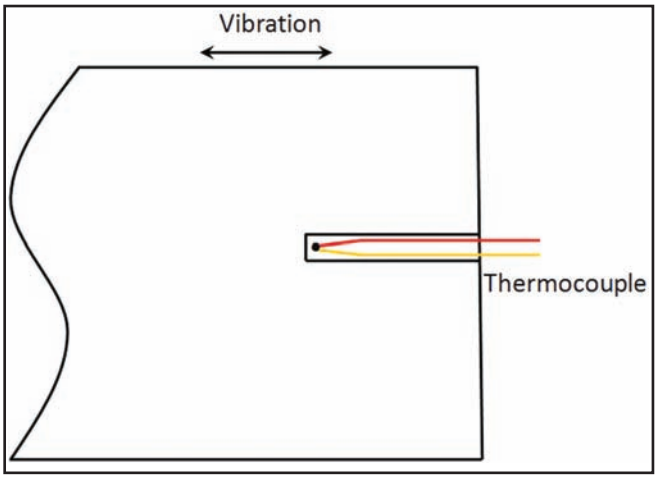

Fig. 2 — Schematic illustration of the top view of the bottom sheet, showing the location of a thermocouple for monitoring the interface temperature change during USW.

USW was reported to reach a peak temperature ranging 35~65% of melting point of the material. Siddiq and Ghassemieh (Ref. 21) explained the ultrasonic welding process of 3003 Al alloy by considering a combined effect of both surface (friction) and volume (plasticity) softening. The coefficient of friction was observed to increase with increasing temperature until a specific temperature, and then decrease.

Furthermore, the previous USW investigations were mainly carried out using relatively thin sheets of up to about 1.2 mm. Since Al alloys possess high electrical and thermal conductivities, the specimen thickness would play an important role in the weldability. It was unknown whether a higher energy input is needed for joining a thicker sheet, how the temperature and microstructure would change during USW, and whether the failure mode would remain the same. The present study was, therefore, aimed at examining the temperature change profile during USW and identifying the effect of welding energy on the tensile shear strength of 2-mm-thick 5754 Al-alloy sheet, which is a typical thickness used in automotive structures.

Experimental Procedure

Ultrasonic spot welds were made on a 2-mm-thick wrought 5754-O Al-alloy sheet, with the nominal composition listed in Table 1 (Ref. 22). The sheet was cut into 80 ×15 × 2-mm test coupons. The length of the coupons was parallel to the rolling direction. The surface of the coupons was prepared by grinding in the direction perpendicular to the coupon length using #80 emery papers, which gave rise to an estimated surface roughness (R_a) of about 140 nm.

The test coupons were overlapped for 20 mm along the length direction, forming an overlapped area of 15 × 20 mm^2 for the lap welding, as shown in Fig. 1. The welds were positioned at the center of the overlapped area. The ultrasonic vibration direction during welding was parallel to the longitudinal direction of the test coupon. A dual-head, wedge-reed-type MH2026DWR welding machine from Sonobond, Inc., West Chester, Pa., configured with a power controller was used for the welding experiments. The flat 8 × 5-mm sonotrode tips used in the present study had serrated surfaces with nine parallel ridges (or teeth) to improve gripping of the lapped sheets. The ridges of the sonotrode tips were oriented perpendicular to the vibration direction during welding. The welding experiments were conducted using time mode at a wide range of energy levels from 2250 to ~5800 J at an impedance setting of 8 and a constant clamping force of 1.64 kN. Laser vibrometry was used to measure the amplitude of oscillation at the sonotrode tip, which was about 5~6 µm. The output energy was achieved by adjusting the power and time. Since the present work aimed to investigate the weldability of a thicker Al sheet with USW, a higher energy input was applied at a slightly longer welding time. Indeed, a weld should be made in less than 1 s in automotive production; therefore, further study will be carried out to optimize the processing parameters especially to shorten the welding time.

To determine the temperature profile during USW, a Type K thermocouple (nickel-chromium vs. nickel-aluminum) was carefully placed in between the two sheets to be joined. Since the welding involves ultrasonic vibration or rubbing of sheets with each other, it was difficult to ensure that the tip of the thermocouple stayed perfectly at the correct location. A roller-like effect of the thermocouple wires might take place. In addition, the thermocouple might separate the sheets to be welded. To overcome the above issues caused by the thermocouple wires on the welding process, a small groove parallel to the ultrasonic vibration direction was made on the lower piece of each pair by scratching the surface using a lathe tool with a sharp edge. The width and depth of the groove were about 0.8 and 0.5 mm, re-

Table 1 — Typical Chemical Composition of 5754-O Aluminum Alloy (wt-%)

Element	Cr	Mn	Mg	Al
Composition, wt-%	0.3	0.5	3.1	Bal

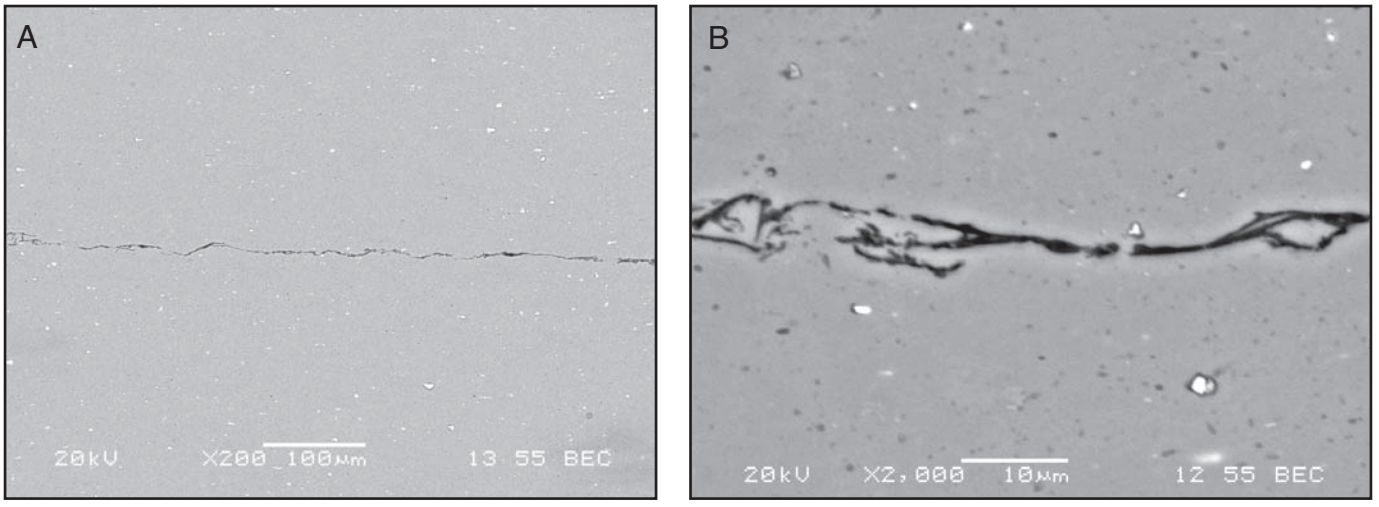

Fig. 4 — A — Lower magnification; B — higher magnification SEM backscattered electron images of the cross section of the spot weld made with a welding energy value of 2580 J.

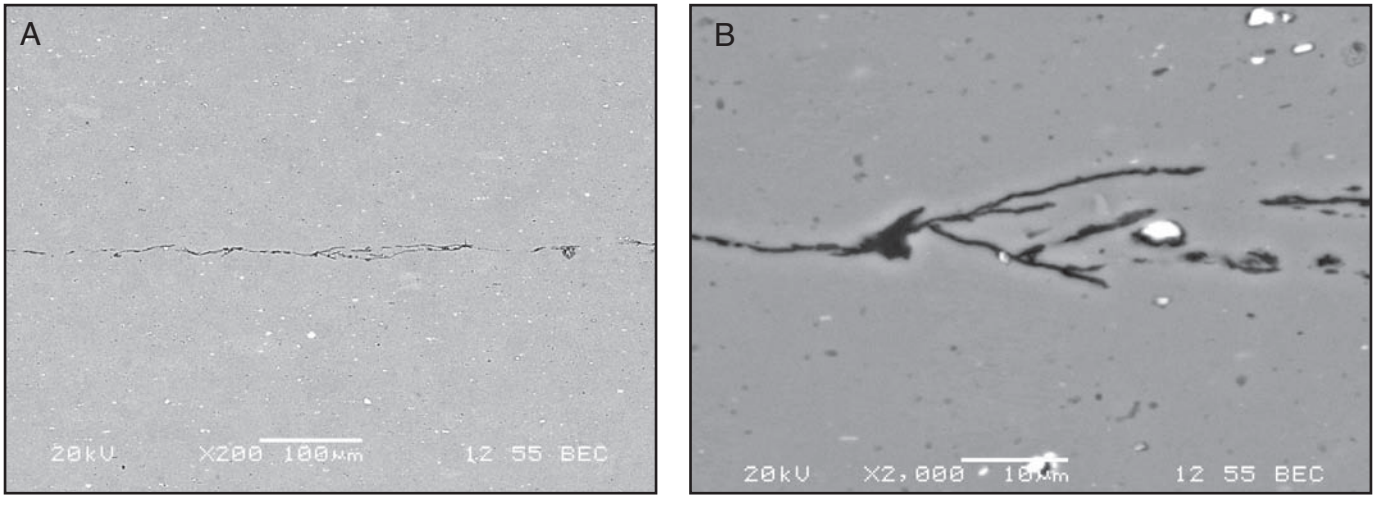

Fig. 5 — A — Lower magnification; B — higher magnification SEM backscattered electron images of the cross section of the spot weld made with a welding energy value of 2839 J.

spectively. The thermocouple wires were laid into the groove with the thermocouple tip located at the center of the weld, as shown in Fig. 2. The signal from the thermocouple during USW was recorded using a computer via a data-acquisition system at a frequency of 50 Hz.

Samples for scanning electron microscopy (SEM) observations were sectioned through the weld nugget parallel to the ultrasonic vibration direction. The sectioned samples were cold-mounted using two-component epoxy resin to avoid any potential microstructural change caused by the hot mounting. The mounted samples were ground with SiC papers up to 1200 ANSI grit, and then polished using diamond paste of 6 and 1 µm followed by alumina paste of 0.3 µm, and finally by vibratory polishing in a colloidal silica of 0.05 µm with a VibroMet® I polisher from Buehler, Lake Bluff, Ill.

To identify an optimum welding condition, tensile shear tests of the ultrasonic spot welds were conducted to evaluate the lap-shear failure load with a computerized United tensile testing machine with a 50-kN load cell at a constant crosshead speed of 1 mm/min at room temperature. During tensile shear testing, restraining shims or spacers were used at both ends of the ultrasonic spot welded samples (Fig. 1) to ensure the alignment and to minimize sheet bending and nugget rotation. The fracture surfaces of the failed samples obtained at various energy levels were then examined via a scanning electron microscope (SEM) equipped with energy-dispersive X-ray spectroscopy (EDS) and three-dimensional (3D) fractographic imaging/analysis capacity.

Table 2 — Comparison of the Weldability of Several Al Alloy Sheets with Various Thicknesses

Material	Processing Parameter	Failure Load	Fracture Mode	Source
1-mm AA6111-T4	Clamping force: 1.9 kN Welding energy: 1500 J Temperature rise: 500°C	3.4 kN	Button pull-out	(Refs. 7, 12)
0.127-mm 1100	Clamping: 0.4 kN Power: 300 W			(Ref. 20)
0.9-mm AA6111-T4	Not given	3.5 kN	Button pull-out	(Ref. 2)
2-mm 5754	Clamping force: 1.64 kN, Welding energy: 4500~5500 J, Temperature rise: ~500°C	4.7 kN	Partial button pull-out	Present

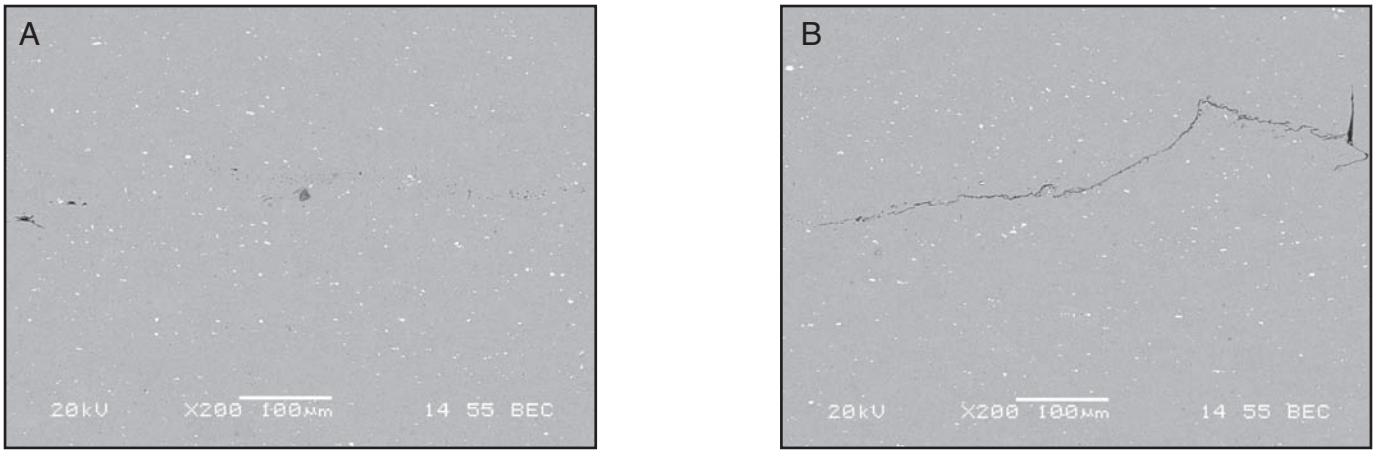

Fig. 6 — SEM backscattered electron images of a joint welded with an energy value of 3242 J. A — In the center of the spot weld; B — near the periphery of the spot weld.

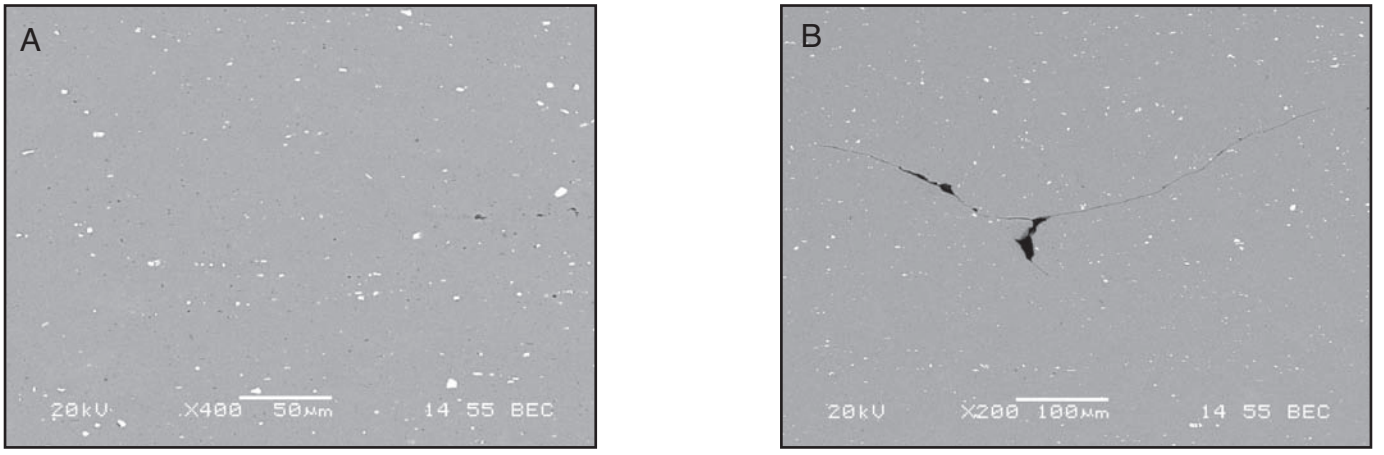

Fig. 7 — SEM backscattered electron images of a joint welded with an energy value of 5287 J. A — In the center of the spot weld; B — near the periphery of the spot weld.

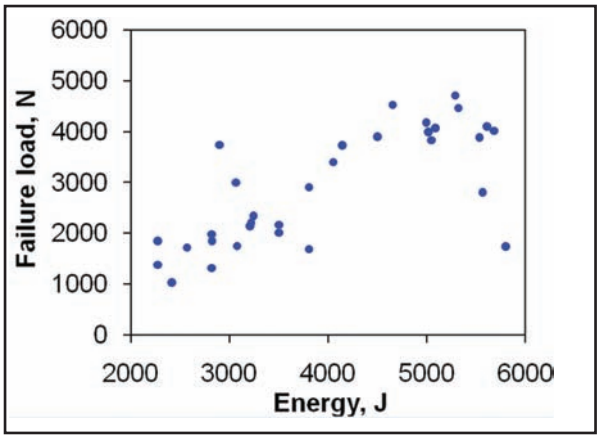

Fig. 8 — Failure load of the tensile lap shear samples welded with different values of welding energy.

Results

Temperature Change

The temperature change during USW, determined using a thermocouple positioned at the center of the weld, is shown in Fig. 3. It is seen that a higher energy input resulted in a higher temperature at the center of the weld. A rapid temperature rise can be seen in the initial stage within about 0.2 s due to the fast rubbing action between the upper and lower roughened-sample surfaces. Then the temperature increase becomes almost linear up to the maximum temperature. The maximum or peak temperature recorded at the end of the welding process was observed to increase from about 186°C with a welding energy of 1624 J to about 420°C, with a welding energy of 3233 J, and to about 535°C with a welding energy of 4995 J. Once the supplied power was off, the sample temperature started to drop rapidly and then slowed during air cooling.

Weld Interface

Figure 4 shows two typical cross-sectional images of the ultrasonic spot welded joints with a lower welding energy (2580 J). A characteristic wavy ultrasonic weld interface can be seen in Fig. 4A. The presence of the wavy weld interface was closely related to the original surface roughness and the applied pressure during USW. As shown in Fig. 4B, bifurcation of the weld interface in some spots can be seen, which was accompanied by localized plastic deformation at the interface. The appearance was typical of that seen in conventional ultrasonic welding at low power (Ref. 23).

The cross section, shown in Fig. 5, is from the joint welded with an intermediate energy of 2839 J. The weld interface becomes discontinuous (Fig. 5A), indicating more extensive plastic deformation and improved weld quality, in comparison to the welded joint made at a lower energy (Fig. 4). However, pores and bifurcation can still be observed, as shown in Fig. 5B. That is, the joining presents like a "tree" at the right-hand side of the image. This kind of tree-like branching is sometimes called "flow" or "wake" features in USW (Ref. 14). Such a discontinuous feature of joining and non-joining appears to disperse randomly over the weld interface — Fig. 5A.

Figure 6 shows SEM images of the

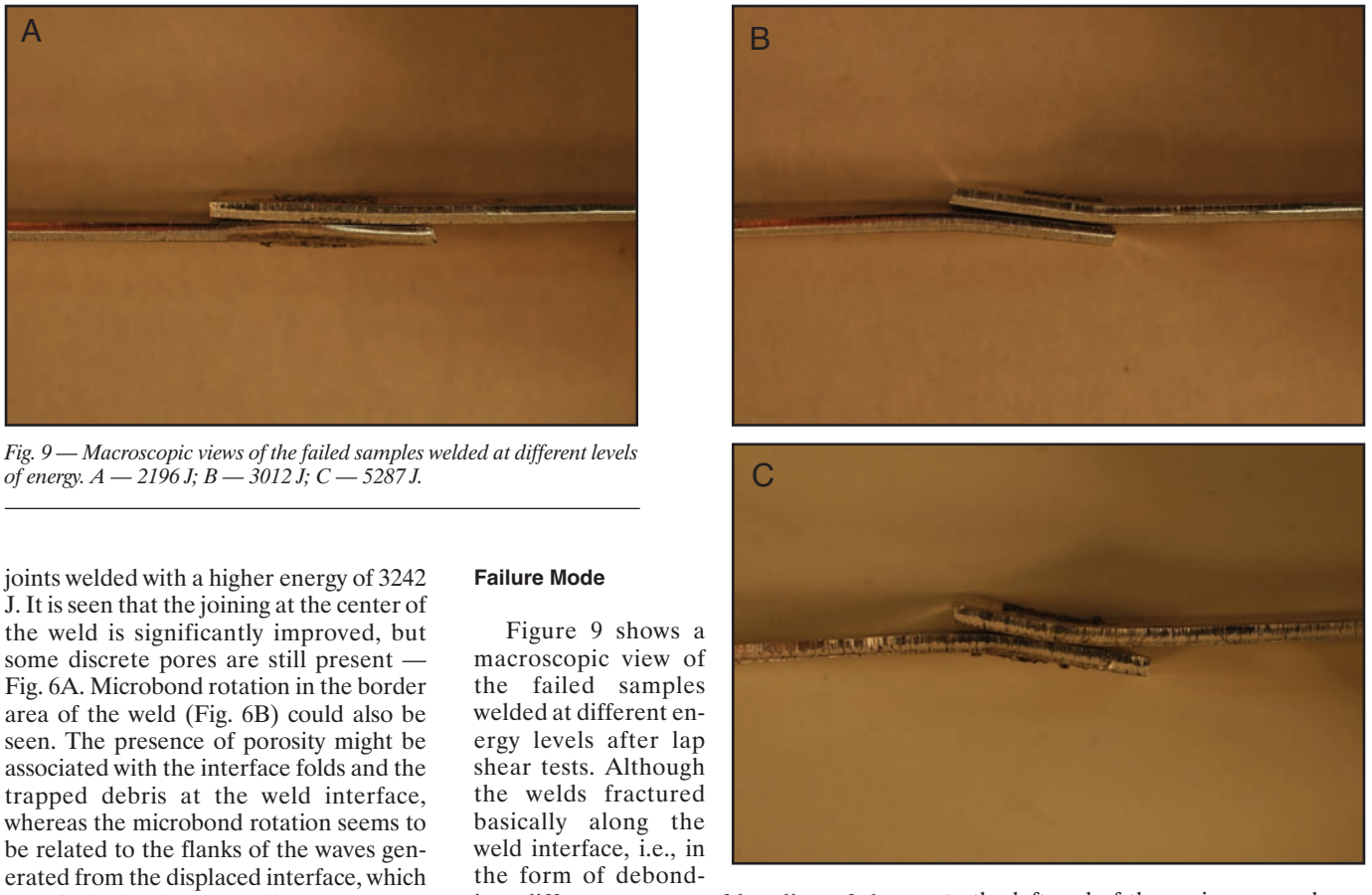

Fig. 9 — Macroscopic views of the failed samples welded at different levels of energy. A — 2196 J; B — 3012 J; C — 5287 J.

joints welded with a higher energy of 3242 J. It is seen that the joining at the center of the weld is significantly improved, but some discrete pores are still present — Fig. 6A. Microbond rotation in the border area of the weld (Fig. 6B) could also be seen. The presence of porosity might be associated with the interface folds and the trapped debris at the weld interface, whereas the microbond rotation seems to be related to the flanks of the waves generated from the displaced interface, which were in the border area of lower pressure, being located in between the sonotrode tips (Ref. 23).

At a further higher level of energy, the interface of the welded joints is essentially not discernible, as shown in Fig. 7A, where an energy value of 5287 J was applied. Therefore, a sound joint is achieved. The border area of the weld is also characterized by the microbond rotation together with branching (Fig. 7B), where the interface rapidly became convoluted and locally displaced by the rotation of the welded segments with some retained porosity.

Lap Tensile Shear Failure Load

The lap shear failure load as a function of welding energy is shown in Fig. 8. It is seen that the failure load first increases and then decreases with increasing welding energy, in spite of the presence of fairly large experimental scatter. The welds produced with an energy level of 4500~5500 J have a high failure load of about 4 kN or higher, with the maximum failure load reaching approximately 4.7 kN, higher than those prepared by resistance spot welding (Refs. 24, 25). When the welding energy exceeds about 5500 J, the lap shear failure load decreases. The change of the failure load with the welding energy is closely related to the welding processes and the related interface features (Figs. 4–7), which will be discussed later. Such a variation trend was also observed in other materials (Refs. 15, 26–28).

Failure Mode

Figure 9 shows a macroscopic view of the failed samples welded at different energy levels after lap shear tests. Although the welds fractured basically along the weld interface, i.e., in the form of debonding, different extents of bending of the failed samples were observed. While the restraining shims were used to maintain the alignment and minimize the rotation of the joints, it is inevitable that the spot weld would inherently experience a rotation. Accordingly, the rotation of the welds could lead to the bending when the sample was loaded in tension gradually. More bending occurred for the samples welded at higher levels of energy. For the weld produced with a lower energy of 2196 J (Fig. 9A), the separated sheets remained almost flat. With increasing welding energy to about 3000 J, a certain extent of bending occurred (Fig. 9B). For the weld made with an energy value of 5287 J, the separated sheets bent significantly, which can be clearly seen in Fig. 9C. The stronger the weld was, the higher the load and plastic deformation were, and the higher the degree of bending was.

Fractography

The typical fracture surface of the joint welded at a low energy level of 2196 J is shown in Fig. 10. Outside the periphery of the weld, a bright zone can be seen, which was identified with EDS to be an oxide layer formed during welding, due to the direct contact of air with the material at an elevated temperature. Just inside the oxide zone there existed a dark zone 2.5~3.0 mm wide, labeled "A" in Fig. 10A, which represents the bonded zone. Close to the left end of the region, several secondary cracks are seen, which occurred during the tensile shear. It suggests that the base material should reach its fracture strength and the fracture initiated in that area. Figure 10B shows a 3D image of the bonded zone. It is seen that the zone was basically flat with a certain amount of ridges at such a low magnification. A magnified image (Fig. 10C) of the bonded zone shows a characteristic dimple fracture, where the elongated dimples indicate the shear fracture via void formation/nucleation, growth, and coalescence. Figure 10D shows the failure mode in the center region of the fracture surface. Apart from some small, isolated dimples and tearing ridges, the predominant feature in the center area is the scrubbing lines parallel to the loading direction. The scrubbing lines are generated due to abrasion or galling of asperities of the microscale roughness of the ground sheet surfaces (Refs. 11, 22).

The dimensions of the welds were observed to remain almost constant, regardless of the change in the welding energy. However, the fraction of the bonded zone increases and the insufficiently bonded center zone decreases, as shown in Fig. 11 for the joint made with a higher welding energy of 5287 J. In the border area at the left end of Fig. 11A, a big crack can be seen in the low-magnification SEM image. The 3D view of the boxed area in Fig. 11A reveals that the crack penetrated into the

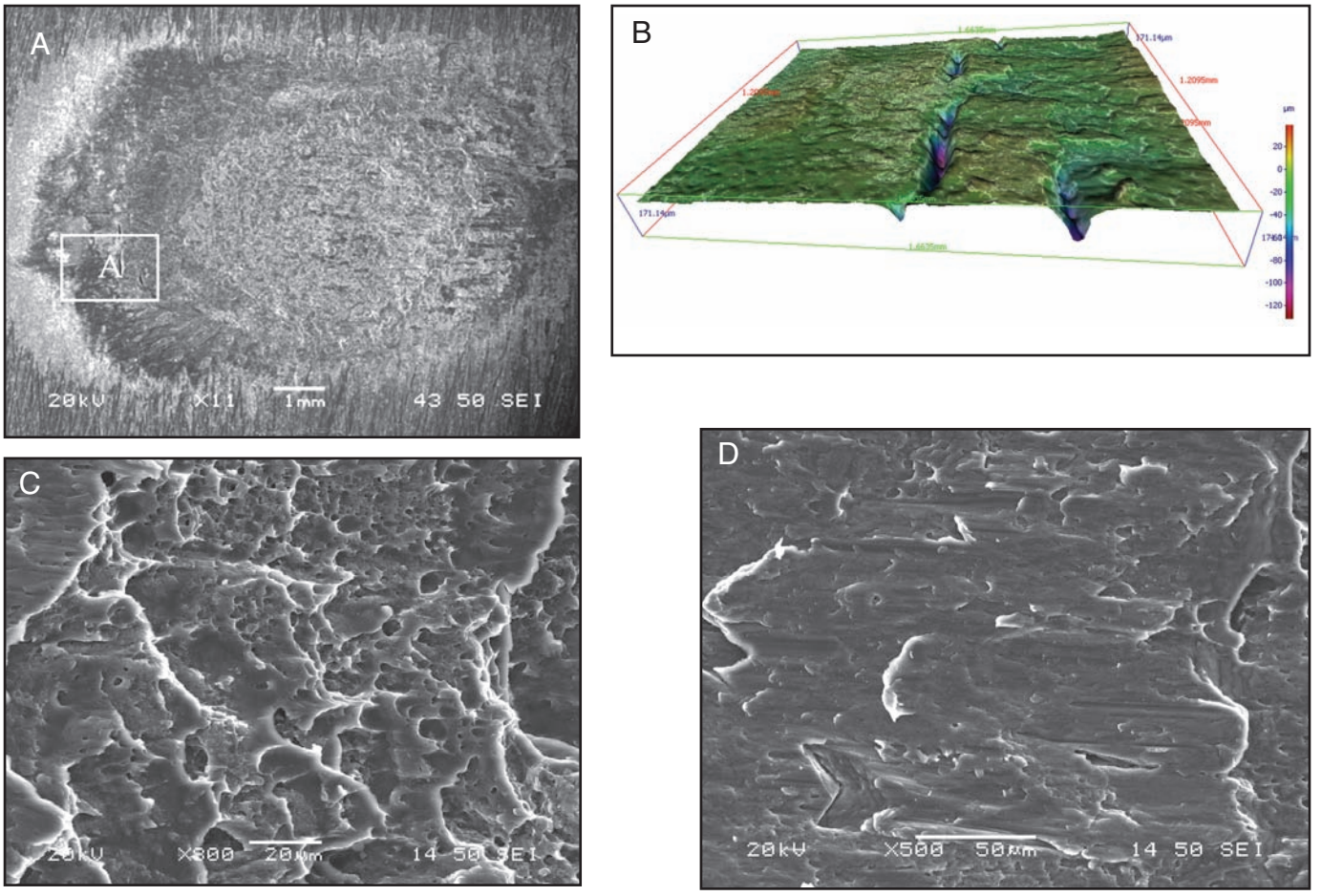

Fig. 10 — Fracture surface of the weld made with an energy value of 2196 J. A — Macroscopic view of the spot weld button; B — 3D view of the bonded zone, marked by "A" in Fig. 10A; C — dimple-rupture failure mode in the bonded zone; D — fracture appearance in the center area of the weld.

material deeply and the crack opening was much larger than that in Fig. 10B. This indeed indicates that the base material was partially pulled out from the weld interface. It should be pointed out that it was possible for the entire weld button to be pulled out for the thinner sheets after USW. For example, the weld button pull-out occurred at a failure load of 3.5 kN for the ultrasonic spot welded 0.9–0.9-mm-thick 6111-T4 Al alloy (Ref. 1). While the ultimate tensile strength of 5754-O Al alloy (220 MPa) was lower than that of 6111-T4 Al alloy (280 MPa) (Ref. 22), the failure loads exceeding 4 kN in the present ultrasonic spot welded 5754-O Al alloy have been achieved when the welding energy lay in between about 4500 and 5500 J — Fig. 8. Nevertheless, no full pull-button failure mode was observed since the thicker, 2-mm sheet was used in this study. The magnified images taken from the well-bonded zone near the periphery (Fig. 11C) and from the center of the weld (Fig. 11D) show the similar failure modes to those seen in Fig. 10C and Fig. 10D. It appears that more dimple-like features and tear ridges occurred in the center area of the weld made at a higher level of energy.

Discussion

The formation of a joint in the ultrasonic welding of metals is a complex process that occurs rapidly under conditions of rubbing action and cyclic deformation at a very high frequency (20 kHz) with a relatively small amplitude arising from the ultrasonic vibration. The high-frequency rubbing action generates friction heat and rapid temperature increase depending on the welding energy applied — Fig. 3. From the cross-section images shown in Figs. 4–7 and the failure load presented in Fig. 8, the quality of the ultrasonic spot welded joints and the tensile shear failure load increased with increasing welding energy up to about 5287 J at which the maximum failure load was achieved. This is a result of the weld area expanding gradually across the weld interface and the rapid softening of the material as the temperature rose more quickly — Fig. 3. During USW, the microscopic cyclic strain amplitude dynamically changed as the weld developed and there was a complex coupling of the sonotrode tips with the sheets, accompanied by acoustic feedback from the parts. Generally, a larger vibration amplitude could be obtained at a higher energy (Refs. 15, 28). The heat could be generated under the sliding between the sheet/sonotrode tip and the sheet/sheet at a high frequency of 20 kHz. However, the specially designed sonotrode tip teeth would crunch into the top and bottom surfaces of both sheets to suppress effectively the generation of high-frequency friction heat between sheet and sonotrode tip. As a result, the heat was predominantly generated in between two sheets to be joined, arising from the high-frequency rubbing action. At a given ultrasonic frequency, the heat generation increased with increasing amplitude of vibration which was dependent on the energy supplied. The higher welding energy led to a faster temperature rise and a higher peak temperature, as shown in Fig. 3. Meanwhile, as the temperature rose, the material was softened. The softening of the material means that the yield strength decreased and the plastic deformation capacity increased. The above effects would cause rapid microjoining, accelerating welding and energy dispersion by plastic work. Obviously, the higher welding energy leading to higher temper-

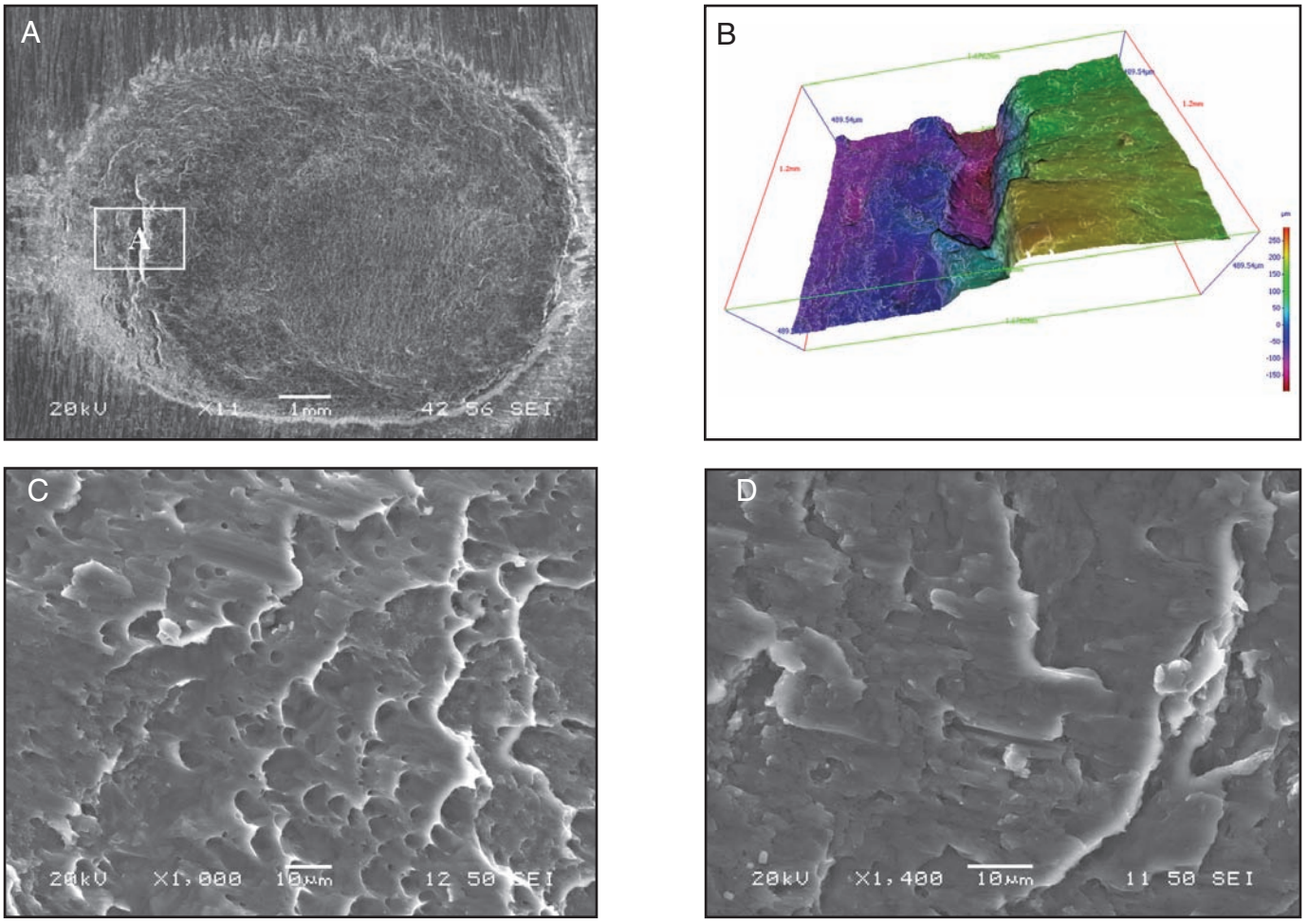

Fig. 11 — Fracture surface of the weld made with an energy value of 5287 J. A — Macroscopic view of the spot weld button; B — 3D view of the bonded zone, marked by "A" in Fig. 11A; C — dimple-rupture failure mode in the bonded zone; D — fracture appearance in the center area of the weld.

atures and more softened material resulted in a better joint, as seen in Figs. 3–8. For example, at an energy level of about 5000 J, a peak temperature of as high as 535°C has been achieved (Fig. 3), resulting in a significant loss of strength and effectively improving the softness since the melting point of this alloy was reported to be about 600°C (Ref. 14). While no high-temperature tensile tests were directly conducted in the present study, other researchers have reported the considerable change of yield strength with the temperature. When temperature increased from room temperature to 371°C, the yield stress fell from 393 to ~28 MPa for 2024-T6 alloy and from 115 to 29 MPa for 5154-O Al alloy (Refs. 22, 29). It was clear that a faster temperature rise and higher peak temperature achieved at a higher level of welding energy corresponded to a higher extent of softness and better plastic deformability, thus enhancing the welding ability of the alloy. As a result, the failure load increases with increasing welding energy. However, if too high energy was used, the resulting larger amplitude of ultrasonic vibration could lead to fatigue damage at the high frequency, whereupon the initial deformation became largely elastic and joining was inhibited (Refs. 15, 28). The optimal welding energy in the present study was observed to be about 5300 J for the 2-mm-thick 5754-O Al sheet — Fig. 8.

Two distinct regions were observed on the fracture surfaces of the ultrasonic spot welded joint: the area near the edge of the weld where joining occurred first and the center where joining only took place at higher welding energies. This behavior could be associated with different stress states on the contacting sheet surface during welding. According to the results of mechanical modeling, there is a nonuniform contact pressure under the sonotrode tips, which is greatest near the periphery of the flat platens (Ref. 20). Then the microjoining occurred first near the edge of the sonotrode tip footprint directly under the sonotrode tip ridge, where the oxide was broken by abrasion, or galling, or asperities resulting from the micron-scale roughness. Figures 10 and 11 confirm that the microjoining indeed started from the periphery area with a slightly higher pressure. Again, as the energy input increased, the temperature between the two sheets being welded increased more rapidly (Fig. 3), and the sheets became more softened, leading to more expanding microjoints toward the center of the weld and a higher lap tensile-shear failure load. However, the subsequent decrease in weld strength (Fig. 8) seen for higher welding energy was related to the increasing penetration of the sonotrode tips into the sheet surfaces, which causes thinning of the weld area.

The above results indicate that the welding quality of the 5754 Al alloy sheets progressively improved. In addition, in agreement with the previous knowledge (Refs. 7, 12), the welding mechanisms of the Al alloy involve solid-state deformation, mechanical interlocking, as well as the formation and progressive spreading of microwelds. The microjoint density increases with increasing welding energy. Therefore, it can be concluded that the weld interface should vary in a similar way for the thin alloy sheet. However, a higher welding energy is required for welding the thicker sheets. This can be seen from Table 2, where the weldability of Al alloys with different thicknesses was summarized. It is clear that a higher welding energy is

needed for welding thicker automotive sheets. For example, a welding energy of the order of 1500 J was required to produce optimized welds in a 1-mm-thick Al sheet that exhibited the desired nugget pull-out failure behavior (Refs. 7, 12). However, the welding energy of 4500~5500 J was needed for the 2-mm-thick 5754 Al alloy sheets in the present work. The maximum failure load was higher than that of the thin sheets and might be higher if the welded joint failed in the manner of full nugget pull-out. Therefore, further attention will be paid to the optimization of the processing parameters for the 2-mm-thick 5754 Al alloy.

Conclusions

1. The temperature at the center of the ultrasonic spot weld increased rapidly at the beginning, and then reached a steady-state linear increase up to a peak temperature at the intermediate and lower energy levels. At higher energy levels, a nonlinear change in the heating rate was observed. When the applied welding energy was about 5000 J, a peak temperature above 500°C was attained, which would considerably soften the material and enhance the joining of the aluminum sheets.

2. The lap tensile shear failure load increased with increasing welding energy up to about 5500 J. When the welding energy was below about 3200 J, the weld interface could be seen and the characteristic tree-like bifurcation appeared at some locations along the weld interface. From 3200 J to about 5000 J, the weld interface was characterized by some discontinuous voids or cracks. When the applied energy lay between about 5000 and 5500 J, the weld interface disappeared and sound spot welds were achieved, corresponding to the maximum level of failure load.

3. Failure occurred basically in a mode of debonding when the spot-welded samples were loaded under tensile shear, but with increasing extent of bending at the weld and partial button pull-out at higher energy levels. This was in line with the higher tensile shear failure load.

4. There existed two distinct regions on the fracture surface. One was the joined region in the vicinity of periphery, and the other was the center region. The joined region was observed to expand gradually to the weld center with increasing welding energy up to about 5500 J.

Acknowledgments

The authors would like to thank the Natural Sciences and Engineering Research Council of Canada (NSERC) and AUTO21 Network of Centers of Excellence for providing financial support. C. Y. Zhang gratefully acknowledges the financial support provided by China Scholarship Council and National Natural Science Foundation of China (No. 51172182), and D. L. Chen is also grateful for the financial support by NSERC-DAS Award, Premier's Research Excellence Award (PREA), Canada Foundation for Innovation (CFI), and Ryerson Research Chair (RRC) program. The authors would like to thank Q. Li, A. Machin, J. Amankrah, C. Ma, R. Churaman, X. J. Zhao, and R. D. Ni for their assistance in the experiments. The authors are also grateful to General Motors Research and Development Center (Warren, Mich.) for supplying the sheet material used in this investigation.

References

1. Hetrick, E. T., Jahn, R., Reatherford, L. V., Ward, S. M., Wilkosz, D. E., Skogsmo, J., Devine, J., Graff, K., and Gehrin, R. 2005. Ultrasonic spot welding: A new tool for aluminum joining. *Welding Journal* 84(2): 26 to 30.

2. Hetrick, E. T., Baer, J. R., Zhu, W., Reatherford, L. V., Grima, A. J., Scholl, D. J., Wilkosz, D. E., Fatima, S., and Ward, S. M. 2009. Ultrasonic metal welding process robustness in aluminum automotive body construction applications. *Welding Journal* 88(2): 149-s to 158-s.

3. Gould, J. E. 2012. Joining aluminum sheet in the automotive industry — A 30 year history. *Welding Journal* 91(1): 23-s to 34-s.

4. Owa, T., Kondo, T., and Takizawa, H. 2010. Production and bond strength of similar-titanium ultrasonic welded joints. *Welding International* 24: 182–187.

5. Zhang, C., and Li, L. 2009. A coupled thermal-mechanical analysis of ultrasonic bonding mechanism. *Metallurgical and Materials Transactions B* 40(2): 196–207.

6. Patel, V. K., Bhole, S. D., and Chen, D. L. 2012. Improving weld strength of magnesium to aluminium dissimilar joints via tin interlayer during ultrasonic spot welding. *Science and Technology of Welding and Joining* 17: 342–347.

7. Chen, Y. C., Bakavos, D., Gholinia, A., and Prangnel, P. B. 2012. HAZ development and accelerated post-weld natural ageing in ultrasonic spot welding aluminium 6111-T4 automotive sheet. *Acta Materialia* 60: 2816–2828.

8. Sriraman, M.R., Babu S. S., and Short, M. 2010. Bonding characteristics during very high power ultrasonic additive manufacturing of copper. *Scripta Materialia* 62: 560–563.

9. Carboni, M., and Moroni, F. 2011. Tensile-shear fatigue behavior of aluminum and magnesium lap-joints obtained by ultrasonic welding and adhesive bonding. *Procedia Engineering* 10: 3561– 3566.

10. Gunduz, I. E., Ando, T., Shattuck, E., Wong, P. Y., and Doumanidis, C. C. 2005. Enhanced diffusion and phase transformations during ultrasonic welding of zinc and aluminum. *Scripta Materialia* 52: 939–943.

11. Daniels, H. P. C. 1965. Ultrasonic welding. *Ultrasonics* 3(4): 190–196.

12. Panteli, A., Robson, J. D., Brough, I., and Prangnell, P. B. 2012. The effect of high strain rate deformation on intermetallic reaction during ultrasonic welding aluminium to magnesium. *Materials Science & Engineering A* 556: 31–42.

13. Jahn, R., Cooper, R., and Wilkosz, D. 2007. The effect of anvil geometry and welding energy on microstructures in ultrasonic spot welds of AA6111-T4. *Metallurgical and Materials Transactions A* 38(3): 570–583.

14. Bakavos, D., and Prangnell, P. B. 2010. Mechanisms of joint and microstructure formation in high power ultrasonic spot welding 6111 aluminium automotive sheet. *Materials Science and Engineering A* 527(23): 6320–6334.

15. Tsujino, J., Sano, T., Ogata, H., Tanaka, S., and Harada, Y. 2002. Complex vibration ultrasonic welding systems with large area welding tips. *Ultrasonics* 40(1): 361–364.

16. Ram, G. D. J., Yang, Y., and Stucker, B. E. 2006. Effect of process parameters on bond formation during ultrasonic consolidation of aluminum alloy 3003. *Journal of Manufacturing systems* 25: 221–238.

17. Matsuoka, S., and Imai, H. 2009. Direct welding of different metals used ultrasonic vibration. *Journal of Materials Processing Technology* 209: 954–960.

18. Zhao, J., Li, H., Choi, H., Cai, W., Abell, J. A., and Li, X. 2013. Insertable thin film thermocouples for in situ transient temperature monitoring in ultrasonic metal welding of battery tabs. *Journal of Manufacturing Processes* 15: 136–140.

19. Elangovan, S., Semeer, S., and Prakasan, K. 2009. Temperature and stress distribution in ultrasonic metal welding — An FEA-based study. *Journal of Materials Processing Technology* 209: 1143–1150.

20. Doumanidis, C., and Gao, Y. 2004. Mechanical modelling of ultrasonic welding. *Welding Journal* 83(4): 140-s to 146-s.

21. Siddiq, A., and Ghassemieh, E. 2009. Theoretical and FE analysis of ultrasonic welding of aluminum alloy 3003. *Journal of Manufacturing Science and Engineering* 131(4): 041007-1 to 041007-11.

22. Myer, K. 2002. *Handbook of Materials Selection*, Chapter 4. New York, N.Y.: John Wiley & Sons, Inc.

23. Harthoorn, J. L. 1978. Ultrasonic metal welding. PhD dissertation. De Technische Hogeschool Eindhoven, NL.

24. Han, L., Thornton, M., Boomer, D., and Shergold, M. 2011. A correlation study of mechanical strength of resistance spot welding of AA5754 aluminium alloy. *Journal of Material Processing Technology* 211(3): 513–521.

25. Darwish, S. M., and Al-Dekhial, S. D. 1999. Micro-hardness of spot welded (B.S. 1050) commercial aluminium as correlated with welding variables and strength attributes. *Journal of Material Processing Technology* 91(1): 43–51.

26. Hulst, A. P. 1972. Macrosonics in industry 2. Ultrasonic welding of metals. *Ultrasonics* 10: 252–261.

27. Ramarathnam, G., North, T. H., and Woodhams, R. T. 1992. Ultrasonic welding using tie-layer materials. Part II: Factors affecting the lap-shear strength of ultrasonic welds. *Polymer Engineering and Science* 32(9): 612–619.

28. Tsujino, J., Hidai, K., Haseawa, A., Kanai, R., Masuura, H., Matsushima, K., and Ueoka, T. 2002. Ultrasonic butt welding of aluminum, aluminum alloy and stainless steel plate specimens. *Ultrasonics* 40(1): 371–374.

29. Davis, J. R. 1993. *Aluminum and Aluminum Alloys, ASM Specialty Handbook*, Chapter 8. Materials Park, Ohio: ASM International.